ORIGINAL ARTICLE

MicrobiologyOpen Open Access WILEY

Identification and characterization of the cell division protein MapZ from *Streptococcus suis*

Muriel Dresen[1] | Manfred Rohde[2] | Jesús Arenas[3] | Astrid de Greeff[4] | Andreas Nerlich[1,5] | Peter Valentin-Weigand[1]

[1]Institute for Microbiology, Center for Infection Medicine, University of Veterinary Medicine Hannover, Hannover, Germany

[2]Central Facility for Microscopy, Helmholtz Centre for Infection Research, Braunschweig, Germany

[3]Unit of Microbiology and Immunology, Faculty of Veterinary, University of Zaragoza, Zaragoza, Spain

[4]Wageningen Bioveterinary Research, Part of Wageningen University and Research, Lelystad, The Netherlands

[5]Veterinary Centre for Resistance Research, Freie Universität Berlin, Berlin, Germany

Correspondence
Andreas Nerlich & Peter Valentin-Weigand, Institute for Microbiology, Center for Infection Medicine, University of Veterinary Medicine Hannover, Germany.
Email: andreas.nerlich@fu-berlin.de (AN); peter.valentin@tiho-hannover.de (PV-W)

Abstract

Streptococcus suis, an emerging zoonotic pathogen, causes invasive diseases in pigs, including sepsis, meningitis, endocarditis, pneumonia, and arthritis. Importantly, similar pathologies are reported in human *S. suis* infections. In previous work, the locus SSU0375 of *S. suis* strain P1.7 had been identified as a conditionally essential gene by intrathecal experimental infection of pigs with a transposon library of *S. suis*. This study aimed to identify the function of the corresponding gene product. Bioinformatics analysis and homology modeling revealed sequence and structural homologies with the *Streptococcus pneumoniae* mid-cell-anchored protein Z (MapZ) that is involved in cell division in different bacterial species. Indeed, depletion of this locus in *S. suis* strain 10 revealed a growth defect as compared to the wild type. Electron microscopy analysis of the corresponding mutant demonstrated morphological growth defects as compared to the wild-type strain, including an irregular cell shape and size as well as mispositioned division septa. Light microscopy and subsequent quantitative image analysis confirmed these morphological alterations. In the genetic rescue strain, the wild-type phenotype was completely restored. In summary, we proposed that SSU0375 or the corresponding locus in strain 10 encode for a *S. suis* MapZ homolog that guides septum positioning as evidenced for other members of the Streptococci family.

KEYWORDS
cell division, electron microscopy, MapZ, quantitative image analysis, *Streptococcus suis*

1 | INTRODUCTION

Streptococcus suis, an emerging zoonotic pathogen, is a common colonizer of the respiratory tract of pigs. It can cause invasive disease with symptoms such as pneumonia, arthritis, meningitis, endocarditis, and acute sepsis, thereby leading to high economic losses in the pig industry worldwide (reviewed in (Goyette-Desjardins et al.,

2014; Votsch et al., 2018)). Similar pathologies are reported in human *S. suis* infections (Gottschalk et al., 2010; Tang et al., 2006). A Multi-Locus Sequence typing (MLST) scheme has been proposed for the genetic classification of *S. suis* strains (King et al., 2002), and based on the capsule polysaccharide this bacterium can also be classified in serotypes (Okura et al., 2016). Nowadays, there are more than 700 sequence types and up to 33 serotypes. Most of the infections

in swine and humans are caused by serotype 2 strains (Goyette-Desjardins et al., 2014). However, infections with serotype 9 strains are becoming increasingly important in several countries, particularly in Western Europe (Goyette-Desjardins et al., 2014; Schultsz et al., 2012). Besides, the number of antibiotic-resistant strains in _S. suis_ isolates has increased over the past years (Palmieri et al., 2011; Tan et al., 2021). Therefore, new therapeutics against streptococcal infections are needed and cell division proteins might be interesting targets for drug development (Shi et al., 2014).

Bacterial binary fission is achieved by accurate placement of the division machinery (Adams & Errington, 2009). For that, bacteria have evolved different mechanisms to identify the cell middle and to position the division machinery, of which the first component is the tubulin-like protein FtsZ (filamentous temperature-sensitive protein Z) (reviewed in (Mahone & Goley, 2020)). After binding to GTP FtsZ assembles into protofilaments to form a contractile ring, the Z-ring. This ring eventually constricts and gives rise to the newborn cells. Two systems, the nucleoid occlusion, and the Min system, earlier emerged to explain the positioning of the Z-ring or mechanisms to control its formation (Bramkamp & van Baarle, 2009; Rothfield et al., 2005). However, several bacteria lack these systems. In recent years, alternative positive regulatory systems were discovered, including the protein MapZ and the serine/threonine kinase StkP. MapZ was first identified in _Streptococcus pneumoniae_ (Fleurie et al., 2014; Holeckova et al., 2014), but it is conserved in _Enterococcaceae_ and _Streptococcaceae_, the two main families of _Lactobacillales_ (Garcia et al., 2016). MapZ was identified to be a substrate of the Ser/Thr kinase StkP (Manuse, Fleurie, et al., 2016). In newborn cells, MapZ colocalizes with FtsZ at mid-cell before it splits into two rings that are pushed apart by nascent peptidoglycan to the cell equators of the future daughter cells. There MapZ positions the FtsZ ring through direct protein-protein interactions. At the same time, a third MapZ ring positions itself at the constriction site and remains until cell division is completed. Thereby, MapZ serves as a permanent beacon of the cell division site (Fleurie et al., 2014; Holeckova et al., 2014). Recently, Zamakhaeva et al. (2021) showed that in _Streptococcus mutans_ MapZ recognizes peptidoglycan decorated with immature serotype c carbohydrates (SCCs), which is primarily located in the equatorial rings and cell poles. Thus, it is being proposed that immature SCCs could serve as a point of reference for the correct positioning of MapZ during cell division.

The MapZ protein consists of a C-terminal extracellular domain and an N-terminal cytoplasmic domain connected by a transmembrane domain (Manuse, Jean, et al., 2016). The intracellular domain belongs to the intrinsically disordered proteins and directly interacts with FtsZ and liposomes _in vitro_ (Hosek et al., 2020). The extracellular domain is divided into two subdomains separated by a serine-rich flexible linker (SRL). The N-terminal subdomain of MapZ$_{extra}$ and the SRL behave as a pedestal for the function of the C-terminal subdomain, which interacts with peptidoglycan. This C-terminal subdomain includes seven conserved amino acids that are essential for MapZ positioning at the cell equator (Manuse, Jean, et al., 2016).

Furthermore, MapZ acts as a guiding track for treadmilling FtsZ filaments and controls the correct position and angle of the FtsZ ring

(Li et al., 2018). Whether MapZ-FtsZ-interaction is sensitive to FtsZ polymerization needs more evaluation since there are contrary findings in the literature (Feng et al., 2019; Hosek et al., 2020). In contrast to former studies, van Raaphorst et al. (2017) provided evidence that MapZ indeed sets the correct division plane in pneumococci, but it is involved neither in the selection of the division site nor in the accurate timing of Z-ring assembly. Mutants devoid of MapZ show an aberrant cell shape and size with mispositioned division septa, formation of cell clusters, and an increase in generation time (Fleurie et al., 2014; Holeckova et al., 2014).

In a recent study using intrathecal infection of pigs with a transposon library of _S. suis_, the locus SSU0375 was identified as conditionally essential for survival in the blood (Arenas et al., 2020). Its predicted protein sequence shows homologies with the mid-cell-anchored protein Z of _S. pneumoniae_. Therefore, the objective of this work was to analyze whether locus SSU0375 (or its corresponding locus in strain 10) codes for _S. suis_ MapZ.

2 | MATERIAL AND METHODS

2.1 | MapZ _in silico_ analysis

MapZ sequences were extracted from the GenomeNet database KEGG. The sequences were aligned with T-Coffee (Notredame et al., 2000) and the alignment was subsequently visualized using TEXshade (Beitz, 2000b). The schematic topology model of the MapZ protein of _S. suis_ (Figure A2a) was predicted with the TMHMM Server v. 2.0 (http://www.cbs.dtu.dk/services/TMHMM, 18.05.21) and visualized with TEXtopo (Beitz, 2000a). Disordered regions in the protein were predicted using PrDOS (Protein DisOrder prediction System) (Ishida & Kinoshita, 2007) (http://prdos.hgc.jp/cgi-bin/top.cgi, 19.03.21). 3D-homology modeling of the extracellular domain was done using the molecular graphics package UCSF Chimera 1.15 (https://www.rbvi.ucsf.edu/chimera) (Pettersen et al., 2004) and is based on the two known subdomain structures of the extracellular domain of the pneumococcal MapZ protein (2nd9.pdb and 2nda.pdb). Alignment and visualization of the structures were performed with UCSF Chimera.

2.2 | Bacterial strains

The virulent _S. suis_ serotype 2 strain 10 was kindly provided by Smith et al. (1999) (Lelystad). Its isogenic _mapZ_-deficient mutant, hereafter called 10Δ_mapZ_, was constructed by the insertion of a spectinomycin cassette in the corresponding putative _mapZ_ gene (locus tag GPW51_RS02050). The generation of mutants in strain 10 has been previously described (Arenas et al., 2020). In brief, a spectinomycin-resistance cassette and the flanking regions of the _mapZ_ gene were amplified from the genomic DNA of strain 10. A new PCR reaction was performed with the spectinomycin-resistance cassette. The cassette was fused to DNA segments of the flanking genes, which were amplified using primer pairs described in Table A1. The final PCR products were

used to transform strain 10 using a competence peptide protocol (Zaccaria et al., 2014). The resulting transformants were selected on Todd-Hewitt Broth (THB; Bacto™, Becton Dickinson) agar plates supplemented with 100 µg/ml spectinomycin (Sigma-Aldrich), and the correct mutants were identified by PCR. To produce the MapZ protein in the 10Δ*mapZ* mutant, the *mapZ* gene from strain 10, including a chloramphenicol-resistance cassette, was reintroduced on the chromosome (Figure A1a). The resulting strain was called cMapZ. For this, *mapZ* and the flanking genes were amplified from the genomic DNA of strain 10. The PCR product was ligated into the pJET1.2/blunt vector using the CloneJET PCR Cloning Kit (Thermo Fisher Scientific) and introduced into *Escherichia coli* DH5α (Thermo Fisher Scientific) by conventional transformation methods. A chloramphenicol-resistance cassette was included upstream of the *mapZ* gene via *in vivo* assembly cloning (Garcia-Nafria et al., 2016). Plasmids and PCR products were purified by commercial kits (NEB, New England Biolabs) and confirmed by sequencing. Then the genes of interest and the chloramphenicol-resistance gene were amplified again. The resulting amplicon was purified and used to transform 10Δ*mapZ* as previously described (Zaccaria et al., 2014). The transformants were selected on THB agar (Becton Dickinson) plates supplemented with 4 µg/ml chloramphenicol (Carl Roth). All PCR reactions were conducted with Phusion polymerase (New England Biolabs). Positive clones were identified by colony PCR. Bacterial colonies were resuspended in water and then incubated in a microwave for 10 min at 100 W. Regular PCR reactions were performed with HotStartTaq Plus DNA polymerase (Qiagen). All primers used in this study are described in Table A1.

2.3 | Growth experiments

Streptococcus suis strain 10, its 10Δ*mapZ* derivative, and cMapZ were cultured overnight at 37°C on Columbia agar supplemented with 7% (v/v) sheep blood (Thermo Fisher Scientific) under aerobic conditions. For liquid cultures, two to three single colonies were inoculated in a starting culture in THB medium supplemented with the corresponding antibiotic and incubated at 37°C overnight. On the next day, bacterial cultures were adjusted to an optical density of 600 nm (OD_{600}) of 0.001 in fresh THB medium without antibiotics. The OD_{600} was measured every 30 min for 8 h. Growth rates were determined by nonlinear regression curve fit.

2.4 | qRT-PCR

Bacterial strains were prepared as described in 2.3 and grown to an OD_{600} of 0.5. The bacteria were harvested by centrifugation, resuspended in 1 ml ice-cold TRI Reagent (Zymo Research), disrupted by an FastPrep-24™ 5G Instrument (3 × 45 s, speed 6.5 MP Biomedicals) and cooled on ice. RNA was purified using the Direct-zol RNA Miniprep Kit (Zymo Research) following the manufacturer's recommendations including DNAse treatment. On-column DNA digestion was performed with the Qiagen DNAse (Qiagen). An additional DNAse treatment was performed after the RNA isolation with the RNeasy Mini Kit (Qiagen). qRT-PCR was performed as previously described by (Willenborg et al., 2014). Briefly, 2 µg of total RNA were reverse transcribed with 500 ng of Random Primers (Promega) and 200 units of M-MLV RT (Promega). The cDNA samples were diluted at 1:20 in nuclease-free water (Sigma-Aldrich) and stored at −20°C. The qRT-PCR reactions were performed with SYBRGreen Mix (Qiagen) and the Stratagene Mx3005P system (Agilent). The qRT-PCR was carried out under the following conditions: initial denaturation for 20 min at 95°C; 40 amplification cycles of 30 s at 95°C, 30 s at 55°C, 20 s at 72°C; and a melting curve for 1 min at 95°C, 30 s at 55°C and 30 s at 95°C. All tested samples were run in duplicate and "no template controls" and "no-RT" controls were included in all runs. The expression levels of the tested genes were normalized using the *gyrB* gene of *S. suis* as an internal standard. Amplification efficiency was determined for each primer pair using serial dilutions of pooled cDNA. Gene expression was calculated by the ΔC_t method (Livak & Schmittgen, 2001). Used primers are described in Table A1.

2.5 | Electron microscopy

Bacterial strains were prepared as described in 2.3 and grown to an OD_{600} of approximately 0.2. Subsequently, samples were fixed by adding methanol-free formaldehyde (Polysciences) to a final concentration of 5% directly into the culture and stored at 4°C. After washing the samples twice with TE buffer (0.01 M Tris, 1 mM EDTA; pH 6.9), they were adsorbed onto poly-L-lysine coated 12 mm coverslips, left for 10 min, and then fixed with 1% glutaraldehyde for 10 min. After another TE buffer washing step, samples were dehydrated with a graded series of acetone (10%, 30%, 50%, 70%, 90%, and 100%) on ice for 15 min for each dilution. After samples in 100% acetone reached room temperature, they were exposed to critical point drying with liquid CO_2 (Leica CPD300). Subsequently, samples were covered with a gold-palladium film (approximately 10 nm) by sputter coating (Bal-Tec SCD500, Balzers Liechtenstein) before examination in a field emission scanning electron microscope (FESEM) Merlin™ (Carl Zeiss). Images were taken with the in-lens SE-detector at an acceleration voltage of 5 kV.

For ultrathin sections, fixed and TE buffer washed bacteria were osmificated with 1% aqueous osmium tetroxide for 1 h at room temperature, washed with TE buffer, and further dehydrated with a graded series of ethanol (10%, 30%, 50%). The 70% step was performed with 4% uranyl acetate in ethanol overnight. Then, dehydration was completed with 90% and 100% ethanol. Infiltration with the embedding resin LRWhite was performed with 1 part resin/1 part 100% ethanol, 2 parts resin/1 part 100% ethanol, followed by pure resin with several changes. Samples were placed into gelatin capsules, filled with pure resin, and polymerized at 50°C for 2 days. Ultrathin sections were cut with a diamond knife. Sections were collected onto butvar-coated copper grids (300 mesh) and counterstained with 4% uranyl acetate for 4 min. Examination of the samples was done using a transmission electron microscope TEM910 (Carl Zeiss) at an acceleration voltage of 80 kV and calibrated magnifications.

2.6 | Light microscopy and image analysis

Bacterial strains were prepared as described in 2.3 and grown to an OD_{600} of approximately 0.3. Then 2 μl of the bacterial culture were spotted on 1% low-melting agarose (GERBU) pads. The samples were analyzed using a Nikon Eclipse Ti-S microscope (Nikon), equipped with the objective Plan Fluor 100×/1.3. Phase-contrast images for quantification were acquired in a blinded manner in 5–15 randomly picked positions per sample.

For segmentation of bacteria, we used StarDist version 0.6.2 (Schmidt et al., 2018), a deep learning framework based on the popular U-Net architecture to detect and segment individual bacteria. Training data sets were generated by first segmenting a set of training images with the Fiji/ImageJ plugin MicrobeJ (Ducret et al., 2016) and subsequent manual correction of suboptimal masks. Training data were further augmented by 90-degree rotations before training. During the training process additional random horizontal and vertical flips, intensity changes, and addition of Gaussian noise were applied to further augment the training data. All images were normalized by simple percentile-based normalization. Eighty percent of the images were used for training and 20% were used for testing. Input image size was 512 × 512 pixels. Details on network architecture and training parameters are summarized in Table A2. The training was performed on an Nvidia Titan RTX GPU. The created masks were used for quantitative image analysis of bacterial cells with the Python library scikit-image (van der Walt et al., 2014). In total, more than 2000 bacteria per strain were analyzed. In some images, obvious abiotic particles were excluded manually from the analysis. Raw data for length and width measurements are provided in the supplementary datasets S1 and S2 (https://doi.org/10.5281/zenodo.5172241). This experiment was performed at least three times with different biological replicates.

2.7 | Van-FL staining

Bacterial strains 10 and 10Δ*mapZ* were prepared as described in 2.3 and grown until an OD_{600} of approximately 0.2. Then 1 ml of the bacterial culture was transferred into a sterile 1.5 ml Eppendorf tube and 5 μl Vancomycin-FL (stock: 100 μg/ml; Thermo Fisher Scientific) as well as 5 μl vancomycin (stock 100 μg/ml; Carl Roth) were added. The cultures were vortexed and incubated at 37°C for additional 20 min. Afterward, the cultures were centrifuged for 10 min at 1690 ×*g* at 4°C. The pellets were washed with HBSS buffer (Thermo Fisher Scientific), resuspended in PBS buffer (Sigma-Aldrich), and fixed in PBS buffer containing 3% formaldehyde. Bacteria were transferred to poly-L-lysine (Sigma-Aldrich) coated coverslips, mounted with ProLong® Gold Antifade Reagent (Cell Signaling Technology), and stored at 4°C until examination.

Confocal microscopy was performed using a TCS SP5 confocal laser scanning microscope equipped with a 63× 1.40–0.60-NA oil HCX Plan Apochromat objective (Leica). Image stacks with a *z*-distance of 0.13 μm per plane were acquired using a 1-Airy-unit pinhole diameter. Images were deconvolved using Huygens® Essential

20.10 (Scientific Volume Imaging). Maximum intensity projections of 3D-stacks were generated and adjusted identically for brightness and contrast in ImageJ/Fiji (Schindelin et al., 2012).

2.8 | Statistical analysis

Values are expressed as mean ± Standard Deviation (SD) of at least three independent experiments. Growth curves were analyzed via nonlinear regression fit with GraphPad PRISM Software 8.01 for Windows (GraphPad Software). Data in Figure 4 were analyzed using estimation statistics with the DABEST package v0.3.1 (Ho et al., 2019). The generated Cumming plots display the magnitude and robustness of the effect size and its bootstrapped 95% confidence interval (CI).

3 | RESULTS AND DISCUSSION

3.1 | *In silico* analysis of *Streptococcus suis* MapZ

The putative *mapZ* gene of strain 10 had been previously identified as a conditionally essential gene for survival in the blood (Arenas et al., 2020). Alignment of the predicted MapZ protein of strain 10 revealed an overall homology of 40% with *S. pneumoniae* MapZ (UniProtKB Q8DR55) (Figure 1a). The C-terminal region showed a higher identity with pneumococcal MapZ (47%) than the N-terminal region (30%) and the linker region (lower than 30%). Previous works described the relatively low conservation of the linker region as well as the intracellular domain of MapZ within *Enterococcaceae* and *Streptococcaceae* family members (Garcia et al., 2016). Furthermore, the seven amino acids (R429, Y431, N448, Y450. Y470, F471, N474) that were claimed essential for the binding of peptidoglycan (Manuse, Jean, et al., 2016), and consequently the correct positioning of MapZ at mid-cell, were conserved in both proteins (Figure 1a).

In a previous study, *S. suis* MapZ was identified as a substrate of the serine/threonine kinase STK that phosphorylates threonine 66 (T66) (Zhang et al., 2017). Similar phosphorylation of T67, besides threonine 78, was observed in the MapZ protein of *S. pneumoniae* and it was suggested that phosphorylation/dephosphorylation of these residues is important for controlling FtsZ function (Fleurie et al., 2014; Holeckova et al., 2014). Nonetheless, alignment of the MapZ proteins from *S. suis* and *S. pneumoniae* revealed that the second threonine found in the pneumococcal protein is not conserved in *S. suis* (Figure 1a). Both, the seven amino acids important for MapZ positioning as well as the two phosphorylation sites are conserved in *S. mutans* (Li et al., 2018). A sequence alignment of MapZ homologs in an earlier study revealed that the two phosphorylation sites are not highly conserved in Streptococci. Some species include both phosphorylation sites (e.g., *S. pneumoniae*, *S. mutans*), others include only the first (e.g., *S. suis*, *Streptococcus sanguinis*) or the second one (e.g., *Streptococcus pyogenes*, *Streptococcus equi* subsp. *zooepidemicus*) or none of them (e.g., *Streptococcus intermedius*) (Holečková
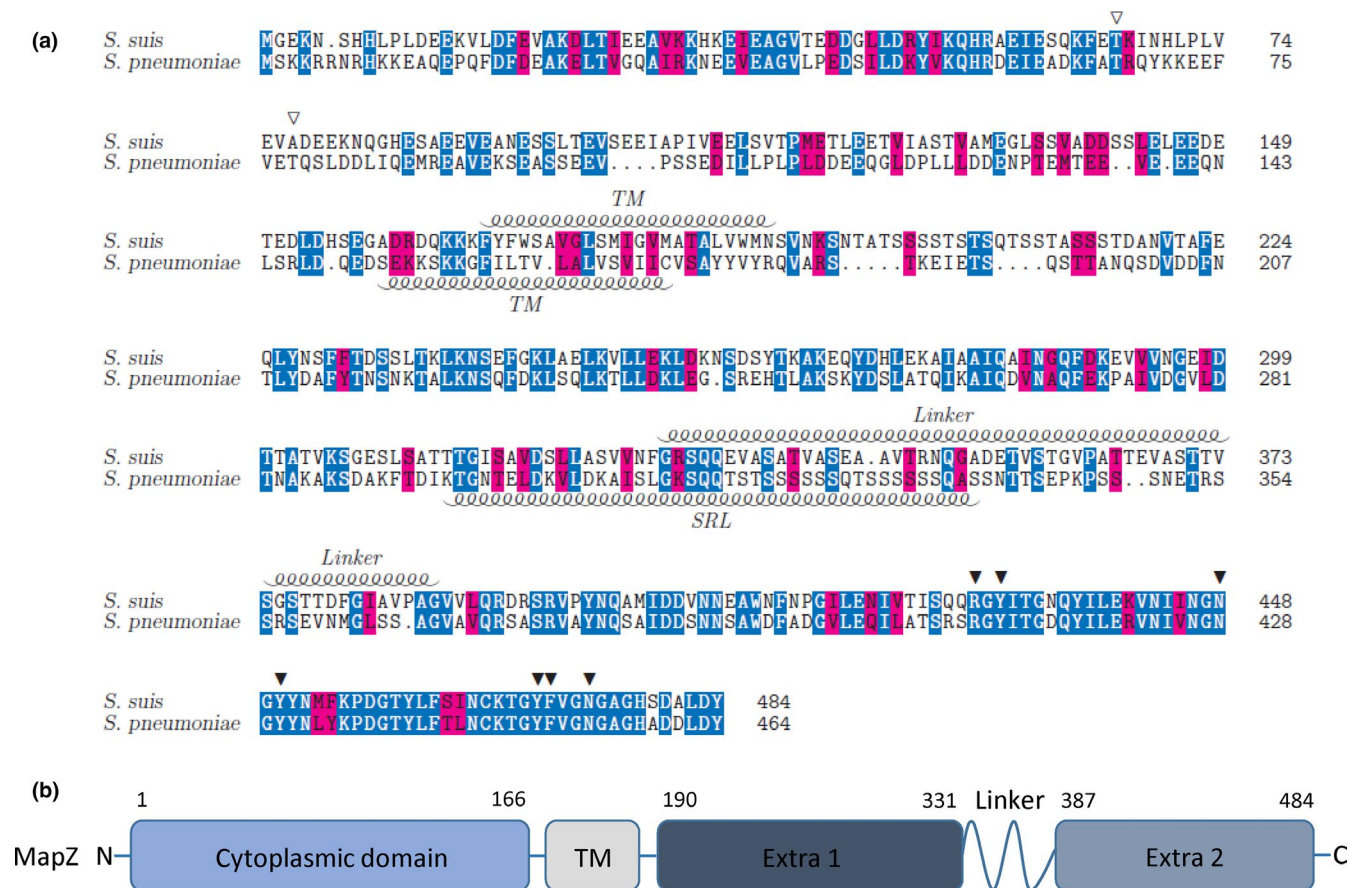
FIGURE 1 *In silico* analysis of the *S. suis* MapZ protein. (a) Alignment of the predicted amino acid sequences of the protein encoded by SSU0375 (locus tag: GPW51_RS02050 in *S. suis* strain 10) and *Streptococcus pneumoniae* MapZ (UniProtKB Q8DR55). The same amino acids are shown in blue, amino acids with a similar function are marked in pink. Closed arrowheads indicate the seven amino acids shown to be essential for the correct positioning of MapZ at mid-cell. Open arrowheads highlight the phosphorylation sites of the pneumococcal MapZ protein. The transmembrane domains (TM), as well as the linker (Linker/SRL) of the two extracellular subdomains, are labeled with a helix. (b) The schematic topological organization model of the predicted MapZ of *S. suis*. The membrane protein is divided into a cytoplasmic domain, a transmembrane domain (TM), and an extracellular domain subdivided into two subdomains (Extra 1, 2) which are separated by a flexible linker. Numbers indicate amino acid positions

et al., 2014). Hosek et al. (2020) described that phosphorylation of MapZ does not affect its structural organization or its interactions with other proteins such as FtsZ. However, the phosphomimetic as well as the phosphoablative form of the pneumococcal MapZ result in cell shape and viability defects. While correct FtsZ positioning is not impaired in these mutants, FtsZ ring structure and numbers are affected (Fleurie et al., 2014). In contrast, Holeckova et al. (2014) did not observe any differences when performing phenotypic analysis of the phosphoablative and the phosphomimetic mutant in comparison to the wild-type strain. In addition, posttranslational modification of the MapZ protein by phosphorylation might play a role in the division process (Bramkamp, 2015). Altogether, the single phosphorylation site of MapZ in *S. suis* seems to be sufficient for proper MapZ function. Besides, the interspecies comparison indicated that there might be different phosphorylation schemes for a functional MapZ protein among Streptococci but its precise function in the different species remains to be analyzed in detail (Holečková et al., 2014).

Despite the reduced homology between *S. suis* MapZ and *S. pneumoniae* MapZ proteins, a comparison of predicted protein topology and structure revealed conservation of the relevant domains with little variation. The linker region in the extracellular domain is predicted to be highly disordered (Figure A2b,c). The domain boundaries in *S. suis* MapZ are indicated in Figure 1b. *Streptococcus suis* MapZ is 20 amino acids longer than *S. pneumoniae* MapZ resulting from different insertions along the domains (Figure 1a, Figure A3a).

Despite the large variability of the extracellular region, the predicted $MapZ_{extra1}$ domain of *S. suis* MapZ is composed of four alpha helices while the $MapZ_{extra2}$ domain is composed of a combination of two small alpha helices and beta strands interconnected with different loops (Figure A3b, Supplementary Movie 1: https://doi.org/10.5281/zenodo.5172241), as described for pneumococcal MapZ using NMR assays. Disordered regions are unable to form stable 3D structures under physiological conditions (Varadi et al., 2014). However, they carry out important cellular functions (Dunker et al., 2002). As our protein predictions are based on homologies to known structures, the tertiary structure of the linker region was not predicted. Intrinsically disordered regions are composed of mainly polar and charged amino acids conferring high flexibility of the respective
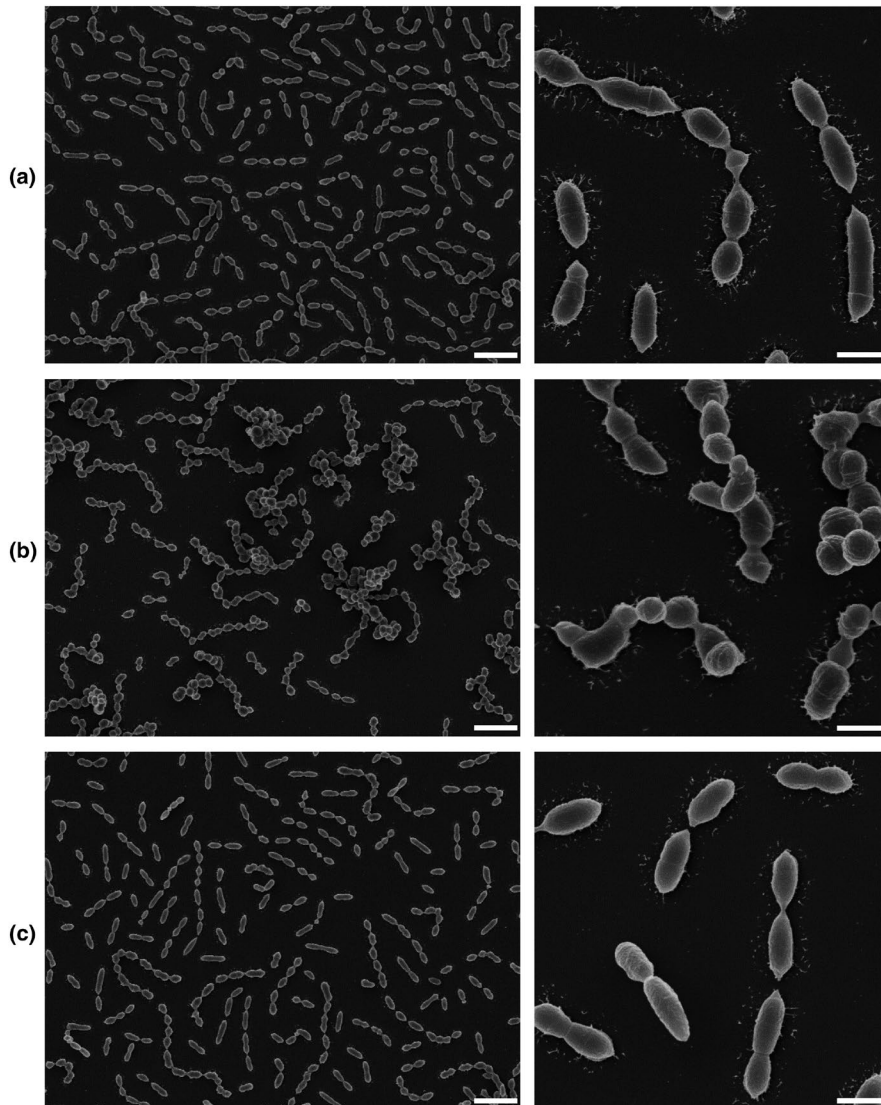
FIGURE 2 Inactivation of _S. suis_ MapZ results in morphological aberrations. Scanning electron microscopy of strain 10 (a), 10Δ*mapZ* (b), and cMapZ (c). Bacteria were grown to the early log-phase, fixed, and processed for electron microscopy. Scale bars represent 4 µm for the left panel and 1 µm for the right panel

region (Xue et al., 2009). They mainly connect the functional domains and generate flexibility between them. Therefore, they often act as domain linkers (Dunker et al., 2002). Consequently, despite the differences in amino acid composition between both MapZ proteins, a disordered linker domain is conserved in _S. suis_, which probably is important for the function or stability of the protein.

In summary, _in silico_ analysis of the protein encoded by the SSU0375 gene locus of _S. suis_ suggests that this is a MapZ homolog to the pneumococcal MapZ protein.

3.2 | Inactivation of MapZ results in cell division defects and septum misplacement

Our _in silico_ studies suggested that SSU0375 codes for _S. suis_ MapZ. To further demonstrate the protein identity, we studied the associated phenotype. Diverse studies on MapZ homologs in other streptococcal species revealed morphological growth defects in mutants lacking MapZ (Fleurie et al., 2014; Li et al., 2018). Therefore, we performed growth experiments and microscopic analysis of strain 10 and

its isogenic mutant 10Δ*mapZ*. Growth experiments revealed a longer lag phase and a reduced growth rate of the mutant compared to the wild type. On the chromosome, _mapZ_ is placed in an operon. Thus, we wondered whether the observed phenotype could be derived from alterations in flanking genes. To prove that, we tested the gene expression of _mapZ_ and its flanking genes using qRT-PCR assays. The results showed alteration of _mapZ_ expression but not of flanking genes (Figure A1b). We then wanted to complement the observed phenotype by reintroducing the _mapZ_ gene on the chromosome of 10Δ*mapZ*. RT-qPCR assays of strain cMapZ showed restoration of _mapZ_ expression (Figure A1b) and observed growth defects (Figure A1c). A similarly reduced growth rate was reported for the pneumococcal Δ*mapZ* mutant (Fleurie et al., 2014; Holeckova et al., 2014) and _S. mutans_ (Li et al., 2018). Accordingly, we concluded that the observed phenotypes are caused by the defects in MapZ production.

To investigate the morphology of the different strains, bacteria grown to the early logarithmic phase were fixed and analyzed by electron microscopy. Results showed typical elongated ellipsoidal cells for the wild type that divided perpendicular to their long axis into successive parallel planes resulting in the formation of short chains. In

FIGURE 3 Inactivation of MapZ results in mispositioned division septa. Transmission electron microscopy of strain 10 (a), 10Δ*mapZ* (b), and cMapZ (c). Bacteria were grown to the early log-phase, fixed, and processed for further analysis. Scale bars represent 400 nm. Arrowheads indicate division septa
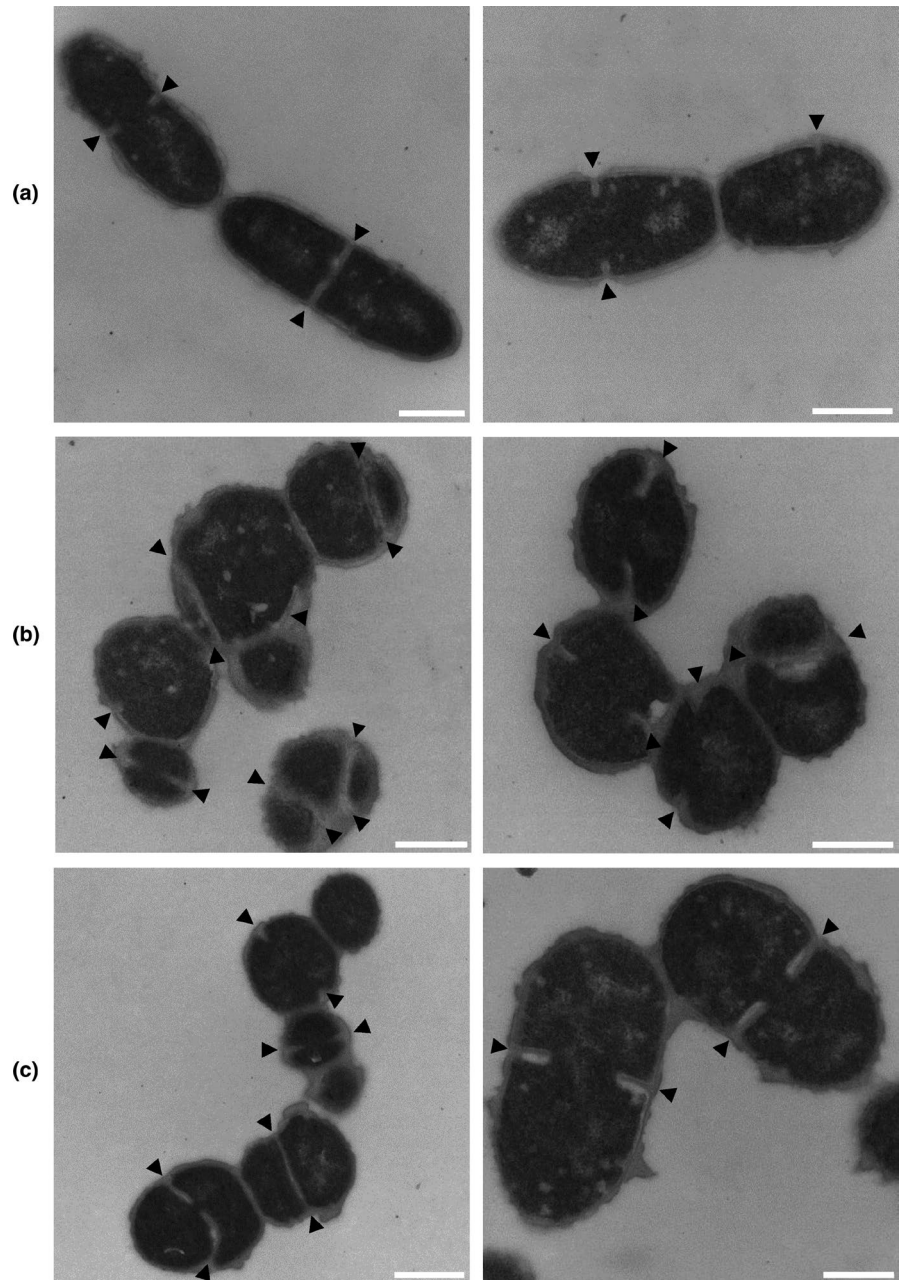

contrast, the MapZ-deficient mutant displayed morphological defects including an irregular cell shape and size of the daughter cells as well as the formation of clusters and small-sized cells (often referred to as minicells; Figure 2). The genetic rescue strain showed a regular cell shape and size comparable to the wild type. Transmission electron microscopy further showed that the division septa were not placed perpendicular to the longitudinal axis in the mutant and that many cells even had several septa located in different axes (Figure 3). These deviations caused a cell division along more than one axis and thereby generated cell clusters. Fleurie et al. reported similar defects for the pneumococcal MapZ mutant (Fleurie et al., 2014). They observed aberrant cell shapes, mispositioned division septa as well as the formation of grape-like clusters (Fleurie et al., 2014). In agreement with our observations, the absence of MapZ in *S. pneumoniae* leads to the formation of minicells that are lacking DNA (Holeckova et al., 2014). The formation

of these unproductive cells may explain a reduced growth rate of the mutant with respect to the wild type. Holečková et al. also reported the presence of multiple division septa in some of the daughter cells (Holeckova et al., 2014), which is in concordance with our observations.

Next, we wanted to quantify these morphological alterations in an unbiased, automatic way. Therefore, we performed a quantitative image analysis. Different cell sizes, morphological changes as well as the formation of aggregates were evident in the MapZ mutant in phase-contrast images while the wild type and the complemented mutant displayed comparable, regular cell shapes (Figure A4). Microscopy pictures were processed via StarDist (Schmidt et al., 2018), a deep learning based application. The mutant showed a slightly reduced cell length with a mean difference of $-0.086\,\mu m$ (95% CI:-0.181, 0.014; Figure 4a), and significantly higher cell width of $0.075\,\mu m$ (95% CI: 0.060, 0.090) than the wild type
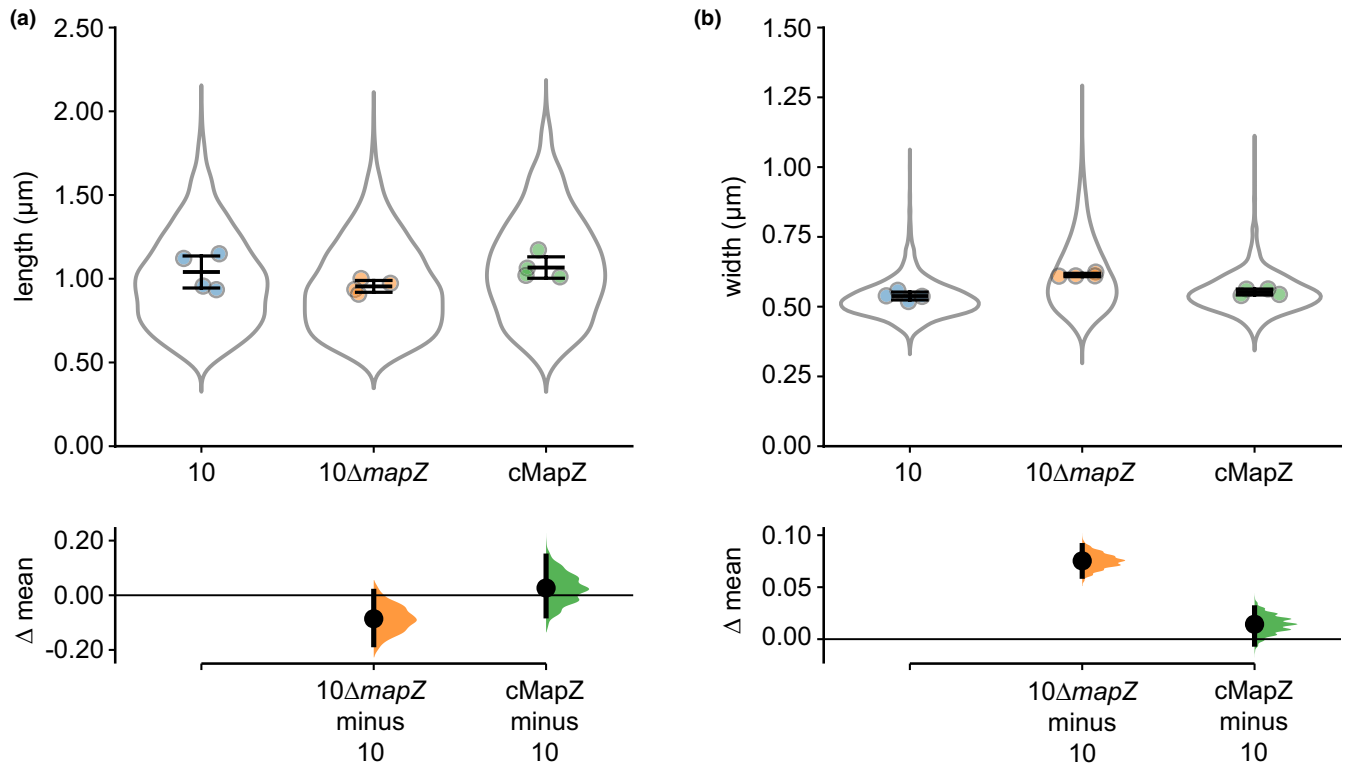
FIGURE 4 Quantitative image analysis of phase-contrast images of strain 10, 10Δ*mapZ*, and cMapZ with StarDist. Results are depicted as Cumming plots. The upper part of the plot shows the mean ± SD of cell length (a) or cell width (b) of four independent experiments. Each dot represents the average of one individual experiment and the violin plot indicates the distribution of all data pooled. The lower part shows effect sizes (Δmean) as dots compared to strain 10 with corresponding bootstrap 95% confidence intervals and resampling distributions of the difference in means
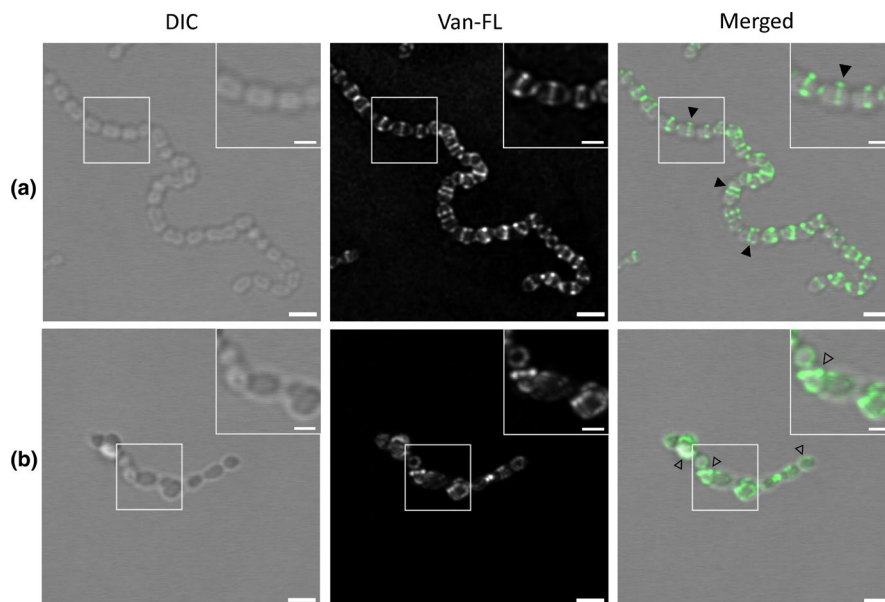
FIGURE 5 Van-FL staining visualizes nascent peptidoglycan synthesis. *Streptococcus suis* strain 10 (a) and 10Δ*mapZ* (b) were grown to the early log-phase and incubated with fluorescent vancomycin for 20 min. Stained cells were analyzed by confocal microscopy. Scale bars represent 2 μm and 1 μm in enlarged insets. Closed arrowheads indicate cell septa located in the middle of the cell; open arrowheads point at fuzzy fluorescent signals

(Figure 4b). The morphology of the strain cMapZ was very similar to the wild type. The mean length difference between these strains was 0.026 μm (95% CI: −0.075, 0.143; Figure 4a) and the mean width difference was 0.014 μm (95% CI: −0.005, 0.030; Figure 4b). Therefore, quantitative image analysis verified our visual interpretations of the electron microscopy assays. Quantitative image analysis

of the pneumococcal MapZ deletion mutants revealed significantly shorter cells compared to the wild type and differences in the cell length distribution (Holeckova et al., 2014). Nevertheless, we could not observe a significant difference between the cell length of the three strains, although indeed we observed minicells in our electron microscopy assays (Figure 2). Probably, the percentage of minicells

in the entire bacterial population is reduced in *S. suis* compared to *S. pneumoniae mapZ* mutants.

In conclusion, the phenotype observed in the *mapZ* mutant is in good agreement with that observed for *mapZ* mutants in other bacteria, confirming that our presumptive *mapZ* gene encodes for MapZ.

3.3 | Van-FL staining visualizes nascent peptidoglycan

Given the conservation of amino acids important for peptidoglycan binding and to further analyze the role of MapZ during septum formation, we stained the bacteria with fluorescently labeled vancomycin (Van-FL) to visualize sites of nascent peptidoglycan synthesis (Daniel & Errington, 2003).

Van-FL staining of *S. suis* strain 10 indicated correct peptidoglycan synthesis and positioning. The cell septa were located at the cell center and perpendicular to the longitudinal axis of the cell (Figure 5a). Although peptidoglycan synthesis was also detected in the corresponding *mapZ* mutant, the staining revealed mispositioned cell septa at an irregular angle and frequently shifted from the cell center. Often only a fuzzy fluorescent signal was detectable (Figure 5b). Similar results were reported for the pneumococcal MapZ-deficient mutant (Holeckova et al., 2014). Thus, the abnormal/misplaced peptidoglycan insertion might be responsible for the abnormal cell division in the mutant strain, which we also observed by electron microscopy. For *S. pneumoniae* van Raaphorst et al. (2017) revealed that the angle of the Z-ring is significantly more skewed in the mutant strain. The authors suggest that MapZ might have a function in cell wall remodeling and maintaining the perpendicular Z-ring plane due to its large peptidoglycan binding domain. Li et al. observed that changes in the angle of the septum mainly occurred during the early formation of the Z-ring and not during its constriction. Thus, the authors conclude that the MapZ protein of *S. mutans* acts as a track for FtsZ filaments only during the early stages of cell division (Li et al., 2018). To underline the results of the Van-FL staining and the electron microscopy, direct labeling of the Z-ring in *S. suis* needs to be addressed in future studies, either by a GFP-fusion or an FtsZ-specific antibody. Thereby not only the positioning but also the angle and structure of the Z-ring can be investigated. This is also interesting in the context of phosphorylation as Fleurie et al. stated effects on FtsZ ring structure and number in phosphomimetic as well as phosphoablative mutants (Fleurie et al., 2014). Altogether, our results confirm previous observations of the pneumococcal MapZ in septum placement and suggest a conserved function within streptococcal species despite the amino acid variability of the protein (Figure 1a). However, the exact mechanism, as well as the role of phosphorylation, need to be elucidated in future studies.

4 | CONCLUSION

In conclusion, our study showed that *S. suis* locus SSU0375 encodes for a homolog of the MapZ protein. As for other streptococci, MapZ is responsible for proper septum placement and is involved in cell division.

The lack of MapZ leads to an increase in generation time as well as morphological growth defects, both causing reduced biological fitness of the mutant *in vivo*, which may explain the necessity of this protein during infection. Previously, cell division proteins have been proposed as interesting targets for drug development (Shi et al., 2014). The physiological role of MapZ in cell division and its demonstrated relevance during infection make this protein a strong candidate for the development of new therapeutics. Future studies will focus on demonstrating how this gene contributes to the survival of *S. suis* in its host and the role of phosphorylation in the function of the MapZ protein.

CONFLICTS OF INTEREST
None declared.

AUTHOR CONTRIBUTIONS
Muriel Dresen: Conceptualization (equal); Formal analysis (equal); Investigation (lead); Writing-original draft (lead); Writing-review & editing (equal). **Manfred Rohde:** Investigation (supporting); Writing-review & editing (supporting). **Jesús Arenas:** Resources (supporting); Writing-review & editing (supporting). **Astrid de Greeff:** Resources (supporting); Writing-review & editing (supporting). **Andreas Nerlich:** Conceptualization (equal); Formal analysis (equal); Investigation (supporting); Software (lead); Supervision (lead); Writing-original draft (supporting); Writing-review & editing (equal). **Peter Valentin-Weigand:** Conceptualization (supporting); Funding acquisition (lead); Supervision (supporting); Writing-review & editing (equal).

ETHICS STATEMENT
None required.

DATA AVAILABILITY STATEMENT
All data generated or analyzed during this study are included in this published article except for the supplementary movie of the homology model, the code for training and analysis of microscopic phase contrast images as well as dataset S1 and S2 that are available in the GitHub repository at https://github.com/AndreasNerlich/Streptococcus_suis_MapZ and in Zenodo: https://doi.org/10.5281/zenodo.5172241.

ORCID
Jesús Arenas https://orcid.org/0000-0002-8134-0693
Astrid de Greeff https://orcid.org/0000-0002-2498-3668
Andreas Nerlich https://orcid.org/0000-0001-8577-2744
*Peter Valentin-Weigand* https://orcid.org/0000-0001-5411-6875

REFERENCES

Adams, D. W., & Errington, J. (2009). Bacterial cell division: Assembly, maintenance and disassembly of the Z ring. _Nature Reviews Microbiology_, 7(9), 642–653. https://doi.org/10.1038/nrmicro2198

Arenas, J., Zomer, A., Harders-Westerveen, J., Bootsma, H. J., De Jonge, M. I., Stockhofe-Zurwieden, N., Smith, H. E., & De Greeff, A. (2020). Identification of conditionally essential genes for S. suis infection in pigs. _Virulence_, 11(1), 446–464. https://doi.org/10.1080/21505594.2020.1764173

Beitz, E. (2000a). T(E)Xtopo: Shaded membrane protein topology plots in LAT(E)X2epsilon. _Bioinformatics_, 16(11), 1050–1051. https://doi.org/10.1093/bioinformatics/16.11.1050

Beitz, E. (2000b). TEXshade: Shading and labeling of multiple sequence alignments using LATEX2 epsilon. _Bioinformatics_, 16(2), 135–139. https://doi.org/10.1093/bioinformatics/16.2.135

Bramkamp, M. (2015). Following the equator: Division site selection in _S. pneumoniae_. _Trends in Microbiology_, 23(3), 121–122. https://doi.org/10.1016/j.tim.2015.02.001

Bramkamp, M., & van Baarle, S. (2009). Division site selection in rod-shaped bacteria. _Current Opinion in Microbiology_, 12(6), 683–688. https://doi.org/10.1016/j.mib.2009.10.002

Daniel, R. A., & Errington, J. (2003). Control of cell morphogenesis in bacteria: Two distinct ways to make a rod-shaped cell. _Cell_, 113(6), 767–776. https://doi.org/10.1016/s0092-8674(03)00421-5

Ducret, A., Quardokus, E. M., & Brun, Y. V. (2016). MicrobeJ, a tool for high throughput bacterial cell detection and quantitative analysis. _Nature Microbiology_, 1(7), 16077. https://doi.org/10.1038/nmicrobiol.2016.77

Dunker, A. K., Brown, C. J., Lawson, J. D., Lakoucheva, L. M., & Obradović, Z. (2002). Intrinsic disorder and protein function. _Biochemistry_, 41(21), 6573–6582. https://doi.org/10.1021/bi012159+

Feng, Z., Zhang, J., Xu, D., Jiang, Y. L., Zhou, C. Z., & Chen, Y. (2019). Multi-functional regulator MapZ controls both positioning and timing of FtsZ polymerization. _Biochemical Journal_, 476(10), 1433–1444. https://doi.org/10.1042/bcj20190138

Fleurie, A., Lesterlin, C., Manuse, S., Zhao, C., Cluzel, C., Lavergne, J.-P., Franz-Wachtel, M., Macek, B., Combet, C., Kuru, E., VanNieuwenhze, M. S., Brun, Y. V., Sherratt, D., & Grangeasse, C. (2014). MapZ marks the division sites and positions FtsZ rings in _S. pneumoniae_. _Nature_, 516(7530), 259–262. https://doi.org/10.1038/nature13966

Garcia, P. S., Simorre, J. P., Brochier-Armanet, C., & Grangeasse, C. (2016). Cell division of _S. pneumoniae_: Think positive! _Current Opinion in Microbiology_, 34, 18–23. https://doi.org/10.1016/j.mib.2016.07.014

García-Nafría, J., Watson, J. F., & Greger, I. H. (2016). IVA cloning: A single-tube universal cloning system exploiting bacterial _in vivo_ assembly. _Scientific Reports_, 6, 27459. https://doi.org/10.1038/srep27459.

Gottschalk, M., Xu, J., Calzas, C., & Segura, M. (2010). _Streptococcus suis_: A new emerging or an old neglected zoonotic pathogen? _Future Microbiology_, 5(3), 371–391. https://doi.org/10.2217/fmb.10.2

Goyette-Desjardins, G., Auger, J. P., Xu, J., Segura, M., & Gottschalk, M. (2014). _Streptococcus suis_, an important pig pathogen and emerging zoonotic agent-an update on the worldwide distribution based on serotyping and sequence typing. _Emerging Microbes and Infections_, 3(6), e45. https://doi.org/10.1038/emi.2014.45

Ho, J., Tumkaya, T., Aryal, S., Choi, H., & Claridge-Chang, A. (2019). Moving beyond P values: Data analysis with estimation graphics. _Nature Methods_, 16(7), 565–566. https://doi.org/10.1038/s41592-019-0470-3

Holečková, N., Doubravová, L., Massidda, O., Molle, V., Buriánková, K., Benada, O., Kofroňová, O., Ulrych, A., & Branny, P. (2014). LocZ is a new cell division protein involved in proper septum placement in _S. pneumoniae_. _MBio_, 6(1), e01700–e01714. https://doi.org/10.1128/mBio.01700-14

Hosek, T., Bougault, C. M., Lavergne, J.-P., Martinez, D., Ayala, I., Fenel, D., Restelli, M., Morlot, C., Habenstein, B., Grangeasse, C., & Simorre, J.-P. (2020). Structural features of the interaction of MapZ with FtsZ and membranes in _S. pneumoniae_. _Scientific Reports_, 10(1), 4051. https://doi.org/10.1038/s41598-020-61036-9

Ishida, T., & Kinoshita, K. (2007). PrDOS: Prediction of disordered protein regions from amino acid sequence. _Nucleic Acids Research_, 35, W460–464. https://doi.org/10.1093/nar/gkm363

King S. J., Leigh J. A., Heath P. J., Luque I., Tarradas C., Dowson C.G., Whatmore A. M. (2002). Development of a Multilocus Sequence Typing Scheme for the Pig Pathogen Streptococcus suis: Identification of Virulent Clones and Potential Capsular Serotype Exchange. _Journal of Clinical Microbiology_, 40(10), 3671–3680. http://dx.doi.org/10.1128/jcm.40.10.3671-3680.2002

Li, Y., Shao, S., Xu, X., Su, X., Sun, Y., & Wei, S. (2018). MapZ forms a stable ring structure that acts as a nanotrack for ftsz treadmilling in _Streptococcus mutans_. _ACS Nano_, 12(6), 6137–6146. https://doi.org/10.1021/acsnano.8b02469

Livak, K. J., & Schmittgen, T. D. (2001). Analysis of relative gene expression data using real-time quantitative PCR and the 2(-Delta Delta C(T)) method. _Methods_, 25(4), 402–408. https://doi.org/10.1006/meth.2001.1262

Mahone, C. R., & Goley, E. D. (2020). Bacterial cell division at a glance. _Journal of Cell Science_, 133(7). https://doi.org/10.1242/jcs.237057

Manuse, S., Fleurie, A., Zucchini, L., Lesterlin, C., & Grangeasse, C. (2016). Role of eukaryotic-like serine/threonine kinases in bacterial cell division and morphogenesis. _FEMS Microbiology Reviews_, 40(1), 41–56. https://doi.org/10.1093/femsre/fuv041

Manuse, S., Jean, N. L., Guinot, M., Lavergne, J.-P., Laguri, C., Bougault, C. M., VanNieuwenhze, M. S., Grangeasse, C., & Simorre, J.-P. (2016). Structure-function analysis of the extracellular domain of the pneumococcal cell division site positioning protein MapZ. _Nature Communications_, 7, 12071. https://doi.org/10.1038/ncomms12071

Notredame, C., Higgins, D. G., & Heringa, J. (2000). T-Coffee: A novel method for fast and accurate multiple sequence alignment. _Journal of Molecular Biology_, 302(1), 205–217. https://doi.org/10.1006/jmbi.2000.4042

Okura, M., Osaki, M., Nomoto, R., Arai, S., Osawa, R., Sekizaki, T., & Takamatsu, D. (2016). Current taxonomical situation of S. suis. _Pathogens_, 5(3), 45. https://doi.org/10.3390/pathogens5030045

Palmieri, C., Varaldo, P. E., & Facinelli, B. (2011). Streptococcus suis, an emerging drug-resistant animal and human pathogen. _Frontiers in Microbiology_, 2, 235. https://doi.org/10.3389/fmicb.2011.00235

Pettersen, E. F., Goddard, T. D., Huang, C. C., Couch, G. S., Greenblatt, D. M., Meng, E. C., & Ferrin, T. E. (2004). UCSF Chimera–a visualization system for exploratory research and analysis. _Journal of Computational Chemistry_, 25(13), 1605–1612. https://doi.org/10.1002/jcc.20084

Rothfield, L., Taghbalout, A., & Shih, Y. L. (2005). Spatial control of bacterial division-site placement. _Nature Reviews: Microbiology_, 3(12), 959–968. https://doi.org/10.1038/nrmicro1290

Schindelin, J., Arganda-Carreras, I., Frise, E., Kaynig, V., Longair, M., Pietzsch, T., Preibisch, S., Rueden, C., Saalfeld, S., Schmid, B., Tinevez, J.-Y., White, D. J., Hartenstein, V., Eliceiri, K., Tomancak, P., & Cardona, A. (2012). Fiji: An open-source platform for biological-image analysis. _Nature Methods_, 9(7), 676–682. https://doi.org/10.1038/nmeth.2019

Schmidt, U., Weigert, M., Broaddus, C., & Myers, G. (2018). Cell Detection with Star-Convex Polygons. _Medical Image Computing and Computer Assisted Intervention – MICCAI 2018. Paper Presented at the International Conference on Medical Image Computing and Computer-Assisted, Intervention. Lecture Notes in Computer Science_ (11071, 265–273). https://doi.org/10.1007/978-3-030-00934-2_30

Schultsz, C., Jansen, E., Keijzers, W., Rothkamp, A., Duim, B., Wagenaar, J. A., & van der Ende, A. (2012). Differences in the population

structure of invasive *S. suis* strains isolated from pigs and from humans in The Netherlands. *PLoS One*, *7*(5), e33854. https://doi.org/10.1371/journal.pone.0033854

Shi, Z., Xuan, C., Han, H., Cheng, X., Wang, J., Feng, Y., Srinivas, S., Lu, G., & Gao, G. F. (2014). Gluconate 5-dehydrogenase (Ga5DH) participates in *S. suis* cell division. *Protein Cell*, *5*(10), 761–769. https://doi.org/10.1007/s13238-014-0074-8

Smith, H. E., Damman, M., van der Velde, J., Wagenaar, F., Wisselink, H. J., Stockhofe-Zurwieden, N., & Smits, M. A. (1999). Identification and characterization of the cps locus of *S. suis* serotype 2: The capsule protects against phagocytosis and is an important virulence factor. *Infection and Immunity*, *67*(4), 1750–1756. https://www.ncbi.nlm.nih.gov/pmc/articles/PMC96524/pdf/ii001750.pdf

Tan, M. F., Tan, J., Zeng, Y. B., Li, H. Q., Yang, Q., & Zhou, R. (2021). Antimicrobial resistance phenotypes and genotypes of S. suis isolated from clinically healthy pigs from 2017 to 2019 in Jiangxi Province, China. *Journal of Applied Microbiology*, *130*(3), 797–806. https://doi.org/10.1111/jam.14831

Tang, J., Wang, C., Feng, Y., Yang, W., Song, H., Chen, Z., Yu, H., Pan, X., Zhou, X., Wang, H., Wu, B. O., Wang, H., Zhao, H., Lin, Y., Yue, J., Wu, Z., He, X., Gao, F., Khan, A. H., ... Gao, G. F. (2006). Streptococcal toxic shock syndrome caused by S. suis serotype 2. *PLoS Med*, *3*(5), e151. https://doi.org/10.1371/journal.pmed.0030151

van der Walt, S., Schönberger, J. L., Nunez-Iglesias, J., Boulogne, F., Warner, J. D., Yager, N., Gouillart, E., & Yu, T. (2014). Scikit-image: Image processing in Python. *PeerJ*, *2*, e453. https://doi.org/10.7717/peerj.453

van Raaphorst, R., Kjos, M., & Veening, J. W. (2017). Chromosome segregation drives division site selection in *S. pneumoniae*. *Proccedings of National Academy of Science of the United States of America*, *114*(29), E5959–E5968. https://doi.org/10.1073/pnas.1620608114

Varadi, M., Kosol, S., Lebrun, P., Valentini, E., Blackledge, M., Dunker, A. K., Felli, I. C., Forman-Kay, J. D., Kriwacki, R. W., Pierattelli, R., Sussman, J., Svergun, D. I., Uversky, V. N., Vendruscolo, M., Wishart, D., Wright, P. E., & Tompa, P. (2014). pE-DB: A database of structural ensembles of intrinsically disordered and of unfolded proteins. *Nucleic Acids Research*, *42*, D326–335. https://doi.org/10.1093/nar/gkt960

Votsch, D., Willenborg, M., Weldearegay, Y. B., & Valentin-Weigand, P. (2018). *S. suis* - The "Two Faces" of a pathobiont in the porcine respiratory tract. *Frontiers in Microbiology*, *9*, 480. https://doi.org/10.3389/fmicb.2018.00480

Willenborg, J., de Greeff, A., Jarek, M., Valentin-Weigand, P., & Goethe, R. (2014). The CcpA regulon of *S. suis* reveals novel insights into the regulation of the streptococcal central carbon metabolism by binding of CcpA to two distinct binding motifs. *Molecular Microbiology*, *92*(1), 61–83. https://doi.org/10.1111/mmi.12537

Xue, B., Li, L., Meroueh, S. O., Uversky, V. N., & Dunker, A. K. (2009). Analysis of structured and intrinsically disordered regions of transmembrane proteins. *Molecular BioSystems*, *5*(12), 1688–1702. https://doi.org/10.1039/b905913j

Zaccaria, E., van Baarlen, P., de Greeff, A., Morrison, D. A., Smith, H., & Wells, J. M. (2014). Control of competence for DNA transformation in S. suis by genetically transferable pheretypes. *PLoS One*, *9*(6), e99394. https://doi.org/10.1371/journal.pone.0099394

Zamakhaeva, S., Chaton, C. T., Rush, J. S., Ajay Castro, S., Kenner, C. W., Yarawsky, A. E., Herr, A. B., van Sorge, N. M., Dorfmueller, H. C., Frolenkov, G. I., Korotkov, K. V., & Korotkova, N. (2021). Modification of cell wall polysaccharide guides cell division in *Streptococcus mutans*. *Nature Chemical Biology*, *17*(8), 878–887. https://doi.org/10.1038/s41589-021-00803-9

Zhang, C., Sun, W., Tan, M., Dong, M., Liu, W., Gao, T., Li, L. U., Xu, Z., & Zhou, R. (2017). The eukaryote-like serine/threonine kinase STK regulates the growth and metabolism of zoonotic *S. suis*. *Frontiers in Cellular and Infection Microbiology*, *7*, 66. https://doi.org/10.3389/fcimb.2017.00066
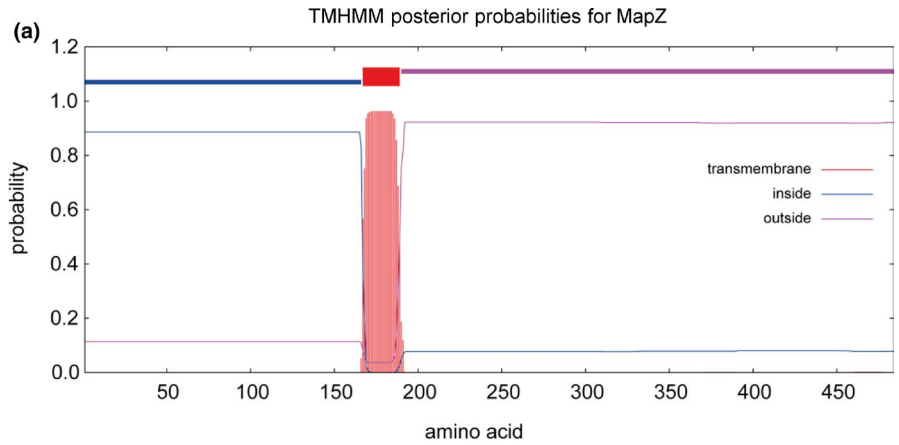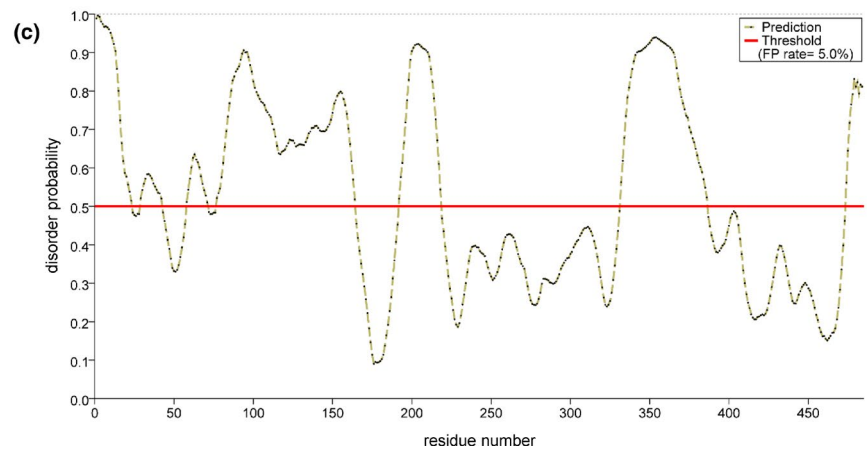
APPENDIX
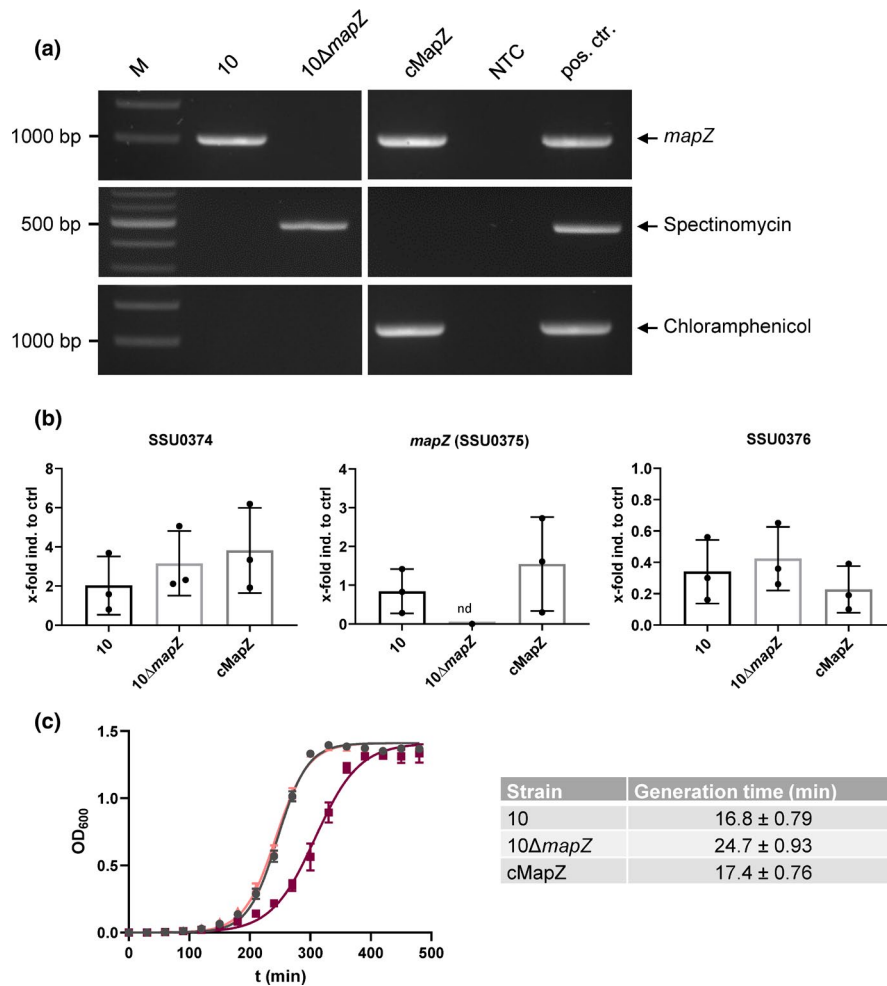
FIGURE A1 Characterization of *Streptococcus suis* mutants by colony PCR, growth in THB media, and qRT-PCR. (a) Amplification of *mapZ* with a fragment size of 1018 bp, genomic DNA served as a positive control, amplification of spectinomycin-resistance cassette with a fragment size of 487 bp, genomic DNA from a *S. suis* strain containing a spectinomycin cassette served as a positive control and amplification of chloramphenicol-resistance cassette with a fragment size of 1018 bp. pSET5s plasmid served as a positive control. Used primers are described in Table A1. (b) The different bacterial strains were grown to the early log phase; RNA was isolated and reverse transcribed followed by qRT-PCR. The expression levels of the tested genes were normalized using the *gyrB* gene of *S. suis* as an internal standard and are presented as x-fold to the control gene. Results show mean ± SD of three independent experiments. nd, not detectable. (c) Growth of S10 wild type (gray), 10Δ*mapZ* (dark red), and cMapZ (light red) in THB media. Starting OD_{600} was adjusted to 0.001. OD_{600} was determined every 30 min for 8 h. The results show a nonlinear regression curve with mean ± SD of three independent experiments. The generation time of the different bacterial strains grown in THB is displayed in the table on the right. Generation time ± SD is shown
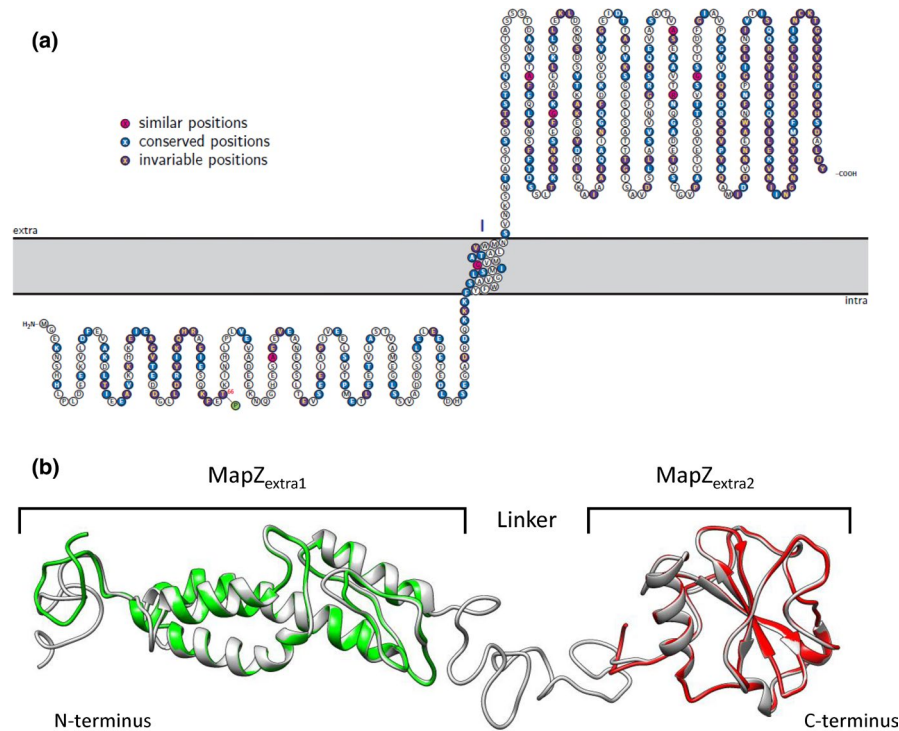
FIGURE A2 Prediction of *Streptococcus suis* MapZ topology. (a) Prediction of topology using TMHMM v2.0. (b) Prediction of disordered regions using PrDOS. Ordered residues are shown in black, disordered residues are in red. (c) Disorder probability of the results in (b). The threshold is indicated by the red line. The analysis was performed with a false positive rate of 5%

(a)

- similar positions
- conserved positions
- invariable positions

extra

intra

(b)

MapZ$_{extra1}$ MapZ$_{extra2}$

Linker

N-terminus   C-terminus

FIGURE A3 Predicted topology and structure of MapZ. (a) Predicted topology of MapZ. MapZ consists of an intracellular domain, a transmembrane domain, and an extracellular domain. Conserved amino acid positions are marked in blue, whereas similar positions are marked in pink. Prediction of membrane protein topology was performed with the TMHMM server and visualization was done with TEXtopo. (b) 3D-homology model of the extracellular domain of MapZ of *Streptococcus suis* based on structures of the pneumococcal protein. Homology modeling was performed with UCSF CHIMERA. The prediction of the MapZ protein of *S. suis* is shown in gray and the two known subdomain structures of the extracellular domain of pneumococcal MapZ in green (2nd9.pdb) and red (2nda.pdb). The extracellular domain of MapZ is divided into two subdomains which are separated by a flexible linker

(a)   **(b)**   **(c)**
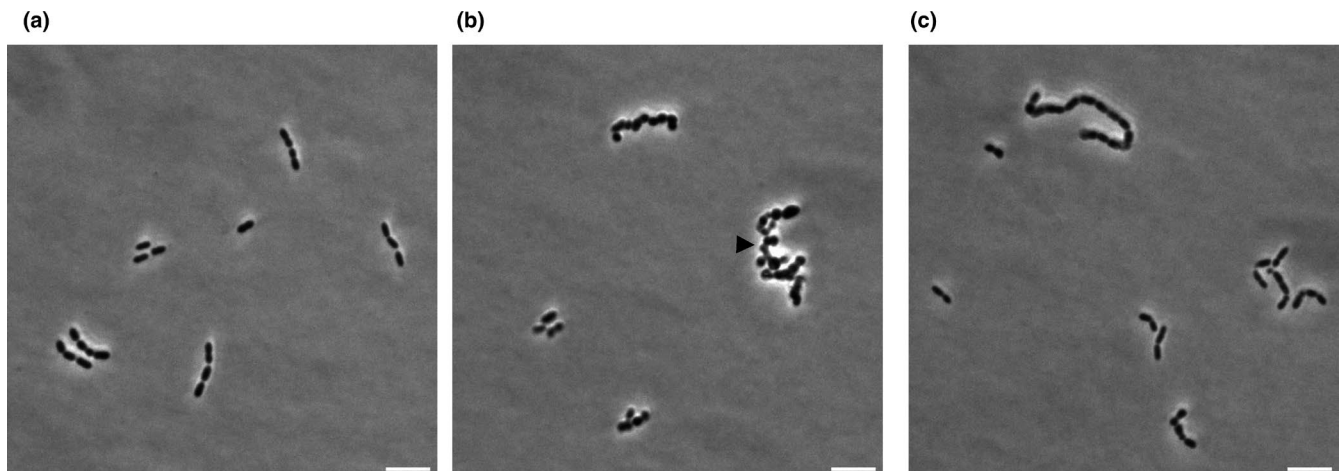
FIGURE A4 Representative phase-contrast images for quantitative image analysis of strain 10 (a), 10Δ*mapZ* (b), and cMapZ (c). The arrowhead indicates cluster formation of the mutant. Scale bars represent 4 μm

TABLE A1 Primers used for mutant construction and characterization

	Purpose	Primer	Sequence (5′–3′)
10Δ*mapz* mutant	First PCR	Fssu0375-L1	CAAGGCCAAATGTGTCAAATC
		Rssu0375-L2	ACGAACGAAAATCGACCTGCTTCGCCACTTCAAAATCTAAAAC
	Second PCR	Fssu0375-R2	TTAGAAAACAATAAACCCTTGCATTTATCAACGGCAATGGCTACTACA
		Rssu0375-R1	ATGGGCTAATCGACTGCTCTCCT
	Amplification of *Spec* cassette	Fspec	GCAGGTCGATTTTCGTTCGT
		Rspec	ATGCAAGGGTTTATTGTTTTCTAA
cMapZ mutant	Cloning of SSU0375 into pJET	SSU0374_for	GTGGGTTGAGGATCAATTGG
		SSU0376_rev	CATCACTTGGGAGGATGTTC
	Plasmid PCR	SSU0375_IVA_pJet_f_2	CCCATCGAATTATCGGAATTTTGGACAATTTCCTTCAATC
		SSU0375_3′_IVA_rev_2	TCGCTGAGATAGGTGCCGAACTTTTTCTTCAATCCGAAGC
	Amplification of *Cm* cassette	CM_for	GGCACCTATCTCAGCGATC
		CM_rev	TCCGATAATTCGATGGGTTCC
	Amplification for transformation	SSU0374_for	GTGGGTTGAGGATCAATTGG
		SSU0376_rev	CATCACTTGGGAGGATGTTC
Colony PCR	Amplification of SSU0375	SSU0375_Seq_for	ACCGAAGACTTGGACCATAG
		SSU0375_SalI_rev_2	GTCGACGCGTTTAATAATCCAAGGCATCAGAATG
	Amplification of *Spec* cassette	Spec_for	AGTCGTCGTATCTGAACC
		Spec_rev	TTCAGCCACTGCATTTCC
	Amplification of *Cm* cassette	CM_for	GGCACCTATCTCAGCGATC
		CM_rev	TCCGATAATTCGATGGGTTCC
qRT-PCR	Amplification of SSU0374	SSU0374_for_qRT	CCAAGTGTGCAGGCTATTTC
		SSU0374_rev_qRT	TGACTGTCGCCACATCTTTC
	Amplification of SSU0375	SSU0375_for_qRT	AAGCCATTGCAGCCATTCAG
		SSU0375_rev_qRT	TGTCGTTGTCGCAGAAAGAG
	Amplification of SSU0376	SSU0376_for_qRT	TGGGCTAATCGACTGCTCTC
		SSU0376_rev_qRT	CTCCCAAGTGATGCCTTCTG
	Amplification of *gyrB*	gyrB_for	GGACCTGGGTGCTTAACAGA
		gyrB_rev	AGGTGGTACCCATGAGCAAG

TABLE A2   Network architecture and training parameters

Parameter	Value
n_rays	32
n_channel_in	1
unet_n_depth	4
unet_kernel_size	[3, 3]
unet_n_filter_base	32
net_conv_after_unet	128
net_input_shape	[None, None, 1]
train_shape_completion	False
train_completion_crop	32
train_patch_size	[256, 256]
train_dist_loss	mae
train_epochs	400
train_steps_per_epoch	100
train_learning_rate	0.0003
train_batch_size	16
train_tensorboard	true
train_checkpoint	weights_best.h5
train_reduce_lr	{'factor': 0.5, 'patience': 40, 'min_delta': 0}